

Investigation of Weld Geometry, Mechanical Properties, and Metallurgical observations of Activated Flux Tungsten Inert Gas (A-TIG) Welding on 304 Austenitic Stainless Steel

Ario Sunar Baskoro¹  · Mohammad Azwar Amat¹ · Agus Widyianto² · Andriawan Dwi Putra¹ · Sinatrya Azali Aryadhani¹

Received: 30 March 2023 / Accepted: 9 November 2023 / Published online: 16 December 2023
© The Indian Institute of Metals - IIM 2023

Abstract The main disadvantage of tungsten inert gas (TIG) welding is the difficulty of getting deep penetration in single-pass TIG welding for plates over 6 mm thick. The activated flux tungsten inert gas (A-TIG) welding method can produce deeper penetration than conventional TIG welding. This study carried out the welding process on stainless steel 304 with the A-TIG welding method. Welding was performed without filler metal (autogenous). The fluxes used are SiO₂, TiO₂, and NSN308. Weld geometry, mechanical properties, and metallurgical observations were conducted to determine the effect of each flux. The results showed an increase in penetration up to 89.9% with SiO₂ flux. In addition, the ultimate tensile strength increased up to 17.2% using flux, but there was a decrease in microhardness in the heat-affected zone region.

Keywords A-TIG · Stainless steel 304 · Weld geometry · Autogenous

1 Introduction

The type of stainless steel that is often used in the manufacturing, food, and automotive industries is stainless steel 304 with austenitic stainless steel (ASS) [1]. Stainless steel has advantages in terms of corrosion and oxidation resistance

and a good combination of strength and ductility [2]. Tungsten inert gas (TIG) welding is an arc welding widely used in industry. TIG welding is used to join metal plates because it allows greater control over the weld, resulting in a more robust and higher-quality weld [2].

The limitations of TIG welding for austenitic stainless steel are due to material thickness, low tolerance for casting variations, and low productivity [3, 4]. To overcome these limitations, activated flux TIG welding (A-TIG) has been developed, which involves using an activating flux to increase the weld penetration achievable at a given current. As a result, a-TIG welding can produce high-quality welds, offers precise heat input control, and has low equipment costs [5].

In a previous study [6], magnets were employed to increase the depth of weld penetration achieved by TIG welding. However, the findings indicate that the form of the welding arc can be altered by applying a magnetic field in the vicinity of the welding torch. Therefore, this will have a knock-on effect on the level of penetration. In addition, several other investigations were conducted to deepen the weld penetration; one of these investigations involved the utilization of activated flux. Coating materials is possible using various activated fluxes, including TiO₂, SiO₂, ZnO, MnO₂, Al₂O₃, AlF₃, CaF₂, CrO₃, and Fe₂O₃ [7, 8].

Activated flux in tungsten inert gas (TIG) welding has been the subject of extensive research, with multiple studies highlighting its benefits and practical uses. A notable investigation by Vidyarthi et al. [9] examined the effects of SiO₂-activated flux on 409 ferritic stainless steel. The analysis provided significant findings showcasing the various advantages of activated TIG (A-TIG) welding. The research findings indicate that A-TIG welding can achieve deeper penetration and reduce angular distortion. This, in turn, leads to enhanced mechanical properties in

✉ Ario Sunar Baskoro
ario@eng.ui.ac.id

¹ Department of Mechanical Engineering, Faculty of Engineering, Universitas Indonesia, Kampus UI, Depok 16424, Indonesia

² Department of Mechanical and Automotive Engineering, Faculty of Vocational, Universitas Negeri Yogyakarta, Kampus Wates, Yogyakarta 55652, Indonesia

the welded joints. The findings mentioned in the text are consistent with observations made by multiple researchers [10–12]. This provides additional support for the improved performance and weld quality that is typically associated with A-TIG welding.

Guilherme et al. [13] conducted a study on austenitic stainless steel 304 and discovered exciting observations about the behavior of the welding arc in A-TIG welding. The study uncovered a significant mention: the occurrence of the welding arc narrowing in A-TIG welding. The narrowing of the weld beads makes them narrower, but it also has the advantage of allowing for deeper penetration into the material. The observation highlights the distinct characteristics of A-TIG welding, emphasizing the importance of precise control over the welding arc. This level of control can result in welds with exceptional penetration depth, offering several benefits in different industrial applications.

The potential of A-TIG welding is being actively explored and harnessed by researchers. In this pursuit, several optimization techniques have been developed to determine the most suitable welding parameters for different situations. The Technique for Order Preference by Similarity to the Ideal Solution (TOPSIS) has been widely recognized as a valuable technique among the mentioned options [14, 15]. The TOPSIS method is helpful for systematically evaluating and selecting welding parameters. It allows researchers and practitioners to adjust their processes to achieve the best possible results carefully. Furthermore, incorporating the heat transfer search algorithm [16] has opened up new possibilities for optimizing welding parameters improving efficiency and accuracy in A-TIG welding procedures.

TIG welding requires a certain current to achieve good penetration depth, but penetration depth can be improved with the A-TIG method by reducing the current. The study compares the mechanical properties and macrostructure of SS 304 stainless steel welded with SiO_2 , TiO_2 , and NSN308 fluxes. Autogenous TIG welding machine parameters are used to obtain results for tensile tests, weld hardness, penetration depth, and bead width.

2 Materials and Methods

The study used a stainless steel SS 304 plate with dimensions of 125 mm \times 50 mm and a thickness of 5 mm. Activated flux variations used were SiO_2 , TiO_2 , and NSN 308, mixed with acetone solution with different ratios, as shown in Fig. 1a. Before applying the activated flux paste, the surface of the specimen was sanded and cleaned. The paste was then smeared with a brush in both vertical and horizontal directions, as shown in Fig. 1b and c.

The study used TIG welding with vertical and horizontal directional welding in specimens. Vertical welding was used for metallurgical and microhardness testing, while horizontal welding was used for tensile testing. The chemical composition of the SS 304 plate tested using an optical emission spectrometer (OES) is shown in Table 1. The welding electrode used was a 2% thoriated tungsten electrode with a diameter of 2.4 mm and a tip angle of 30°. Argon gas was used as a protective gas with a flow rate of 11 L min^{-1} for the upper gas and 3 L min^{-1} for the lower gas [17].

Welding parameters for welding in vertical and horizontal directions are shown in Tables 2 and 3.

Fig. 1 Schematic illustration of **a** mixing of activated flux, **b** dimensions of coating flux for metallurgical, microhardness test, and **c** dimensions of coating flux for tensile test

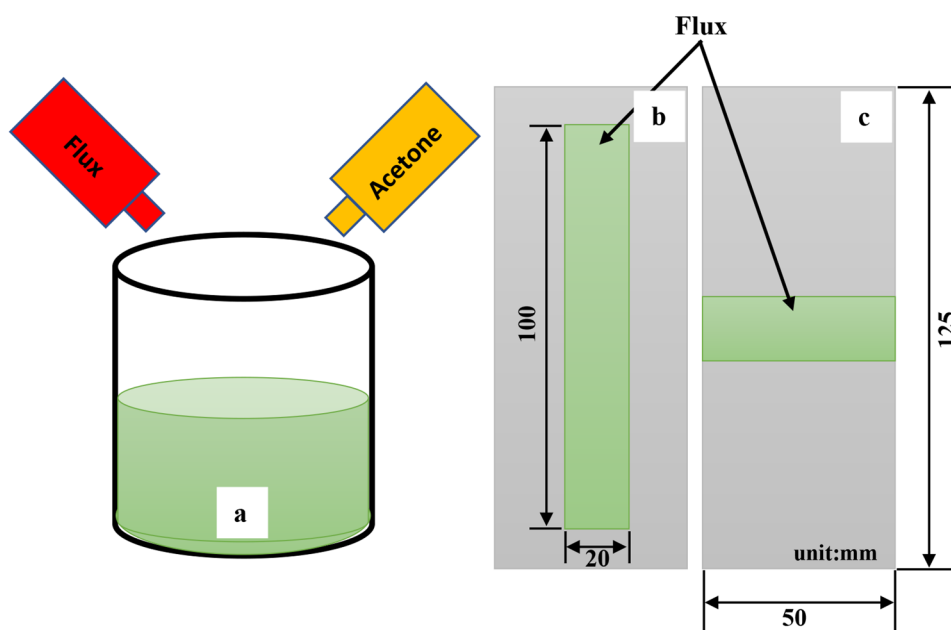


Table 1 Chemical composition of SS 304 plate (wt %)

SS 304	C	Si	Mn	P	S	Cr	Mo
	0.36	0.456	0.906	0.24	<0.05	18.6	0.119
	Ni	Al	Cu	Nb	Ti	V	Fe
	0.91	0.02	0.195	0.08	<0.02	0.73	bal

Table 2 Welding parameters for vertical directional welding

Flux type	Heat input (kJ mm ⁻¹)	Welding current (A)	Welding speed (mm min ⁻¹)	Upper flow rate (L min ⁻¹)
No Flux	0.508	100	120	10
SiO ₂				
TiO ₂				
NSN 308				

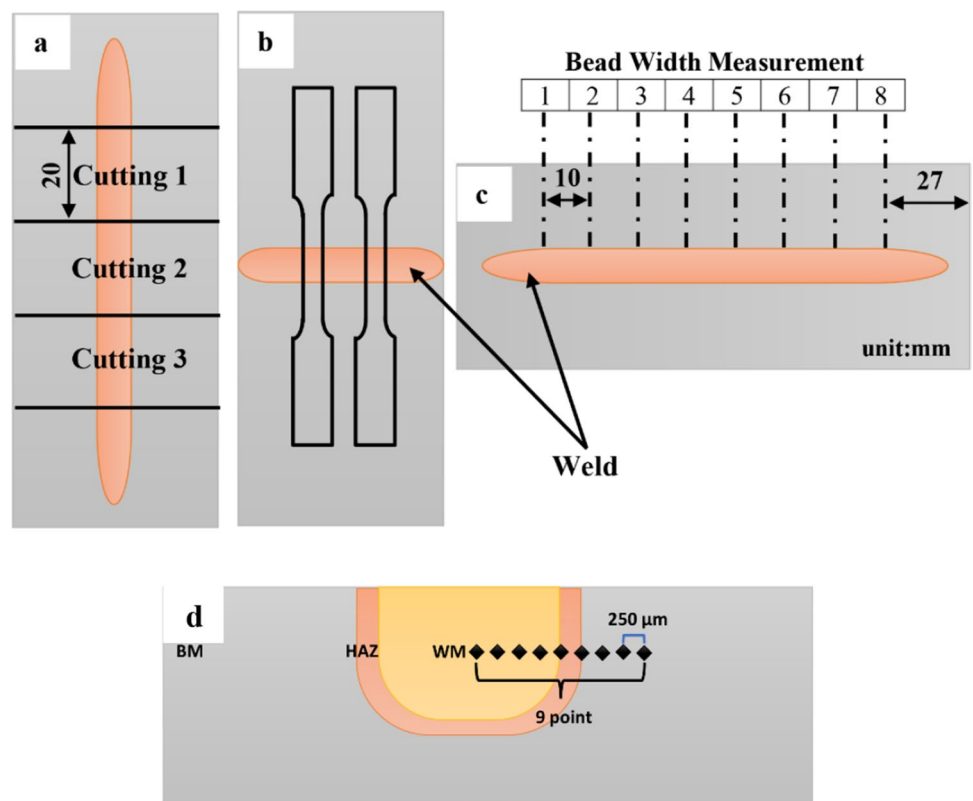
The welding geometry test involves measuring the top bead width, the depth of welding penetration, and the D/W ratio. The top bead width was measured at eight points with a distance of 10 mm, starting from 27 mm from the edge of the specimen. The depth of welding penetration was measured from cutting 1 until cutting 3. A schematic illustration of the top bead width measurement is shown in Fig. 2c. The measurement was done using a digital microscope.

Metallurgical testing includes macrostructure and microstructure observations. The specimens were cut in cross

Table 3 Welding parameters for horizontal directional welding

Flux type	Welding current (A)	Heat input (kJ mm ⁻¹)	Welding speed (mm min ⁻¹)	Upper flow rate (L min ⁻¹)	Backing flow rate (L min ⁻¹)
No Flux	210	1.769	120	11	3
SiO ₂	150	0.870			
TiO ₂	160	0.996			
NSN 308	180	1.310			

Fig. 2 Schematic illustration of top view: **a** metallurgical test, **b** tensile test, **c** bead width measurement, and a cross section of **d** microhardness test



section into three cutting pieces: cutting 1 (25%), cutting 2 (50%), and cutting 3 (75%) pieces, which are shown in Fig. 2a. Macrostructure observations were carried out on one side of the three cutting pieces, while microstructure observations were carried out on cutting 2 (50%). Metallographic testing is to observe the grain structure of a welded product. The specimen was sanded and polished with titanium (IV) oxide and ethanol. An etching solution of HNO_3 , HCl , picric acid, and ethanol was used, and metallographic observations were carried out with the help of digital and optical microscopes. The purpose of the metallography is to measure the depth of penetration and the width of the bead to determine the D/W ratio and to evaluate segregation in different areas of the weld.

Mechanical testing of the weld joint was conducted, including tensile and microhardness tests. The tensile test was conducted according to the ASTM E-8M standard using a universal testing machine. The microhardness was measured using a Mitutoyo 810 Vickers microhardness testing machine with a load of 500 gr for a dwell time of 15 s in three zones of weld joint of weld metal (WM), heat-affected zone (HAZ), and base metal (BM). The microhardness measurements were taken at three points of indentation with a distance of 250 μm per indentation with horizontal distribution, as shown in Fig. 2d.

3 Results and Discussion

3.1 Weld Geometry of TIG and A-TIG Weldment

The weld geometry can be investigated from bead width, penetration depth, and depth/width (D/W ratio). Figure 3 is an example of a specimen using the SiO_2 -activated flux. The weld surface profile of vertical directional welding, horizontal directional welding, and cutting for metallurgical test specimens is shown in Fig. 3a–c, respectively.

Figure 4a and b shows the average top bead width (TBW) and D/W ratio with the activated flux variation. The average TBW is widest in TIG welding without activated flux (5.574 mm) and narrowest in welding with SiO_2 flux (4.436 mm), followed by NSN 308 and TiO_2 fluxes. The largest D/W ratio is found in A-TIG welding with SiO_2 flux (0.088), while TIG welding without flux produces the smallest D/W ratio (0.038). The difference in bead width and depth of penetration between welding without flux and welding with flux is affected by Marangoni convection, as shown in Fig. 6. Marangoni convection will make the welding arc narrower and more pointed when using flux [18]. This phenomenon causes the welding with flux to penetrate deeper but narrower weld beads.

The macrostructure was observed to determine the penetration depth between TIG welding without flux and TIG

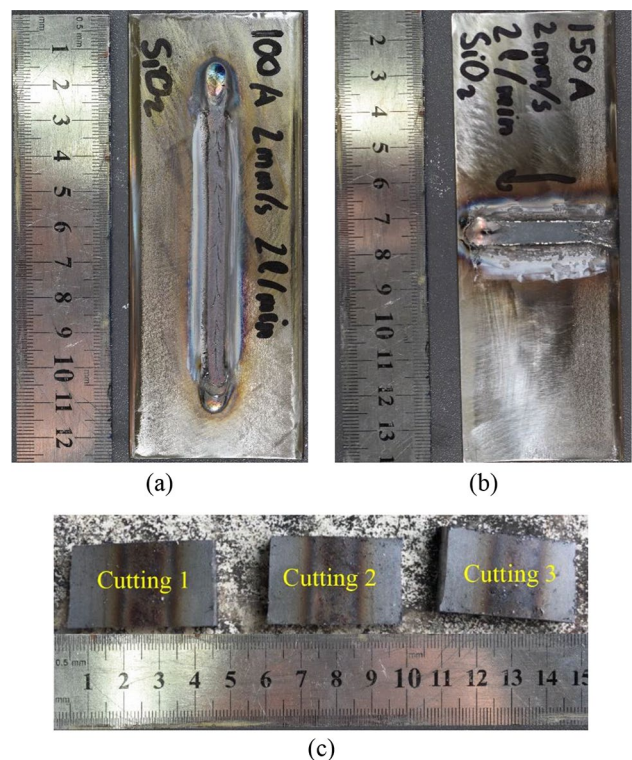


Fig. 3 The weld surface of **a** vertical welding, **b** horizontal welding, and **c** specimens for metallurgical and microhardness test

welding with flux. Observations were made at three weld cross sections: 25, 50, and 75%. For fluxless TIG welding, the average penetration depth is 1.736 ± 0.076 mm. Meanwhile, welding with SiO_2 , TiO_2 , and NSN308 fluxes has an average penetration depth of 3.014 ± 0.722 , 2.641 ± 0.060 , and 2.068 ± 0.064 mm, respectively (see Fig. 5). The addition of activated flux in TIG welding results in deeper weld penetration, with SiO_2 producing the deepest among other types of flux. The penetration depth increases by 89.8% with SiO_2 flux, 47.9% with TiO_2 flux, and 23.5% with NSN308 flux compared to welding without flux. All specimens receive the same heat input of 0.508 kJ mm^{-1} . Other studies also mention that SiO_2 -type fluxes can produce deeper penetration [12, 19].

SiO_2 , a popular flux ingredient in A-TIG welding, greatly aids weld penetration. This is because SiO_2 is effective at concentrating heat in the weld pool. This results in more significant base material melting and fusion, allowing greater penetration into the stainless steel substrate. The enhanced penetration depth is advantageous in situations that call for highly durable weld connections. SiO_2 flux can keep a uniform and steady penetration profile over several welds. This uniformity of weld quality is essential in industrial operations since it dramatically decreases the possibility of faults and guarantees predictable outcomes. SiO_2 flux's ability to improve penetration depth under control is functional when

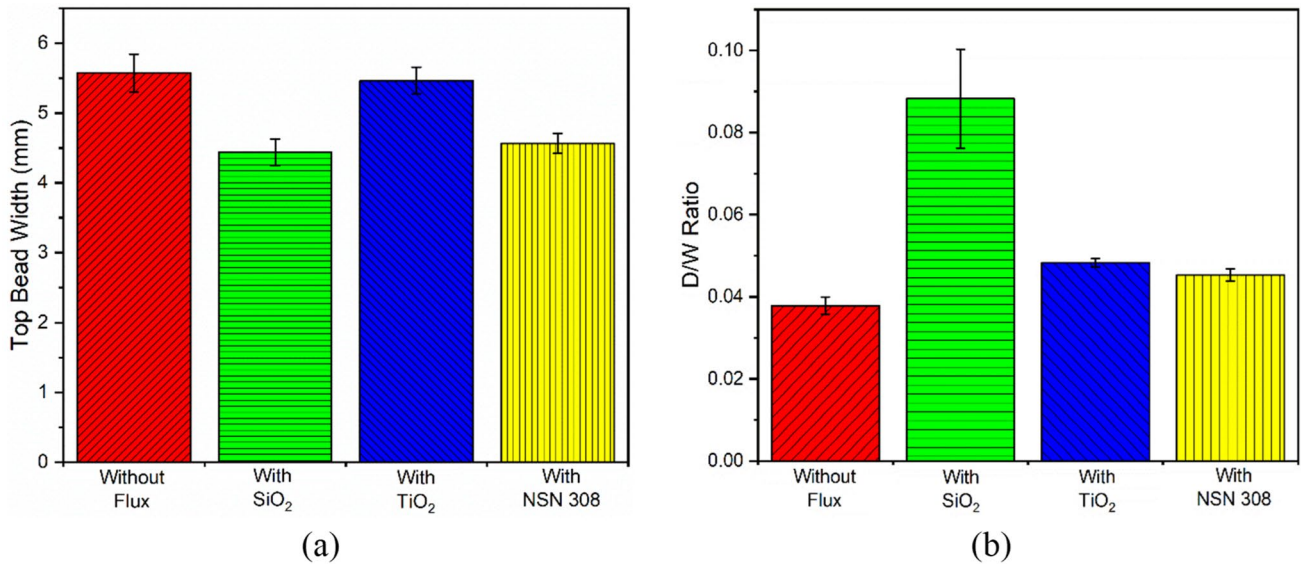


Fig. 4 Weld geometry on various activated flux **a** average of top bead width and **b** average of *D/W* ratio

Flux type	Cutting 1	Cutting 2	Cutting 3	Depth (mm)	D/W
No Flux				1.663	0.036
				1.815	0.040
				1.729	0.037
SiO ₂				2.180	0.076
				3.445	0.101
				3.416	0.088
TiO ₂				2.666	0.048
				2.685	0.049
				2.573	0.048
NSN 308				2.038	0.045
				2.025	0.044
				2.142	0.047

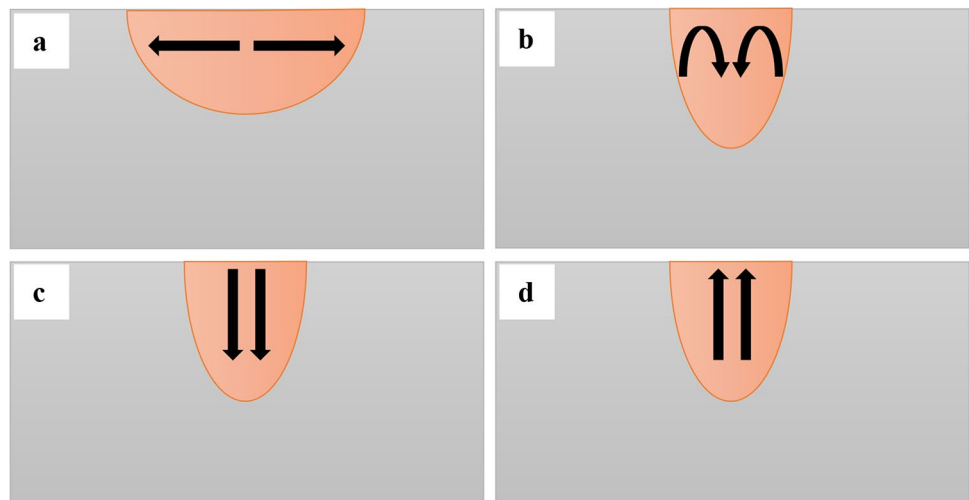
Fig. 5 Macrographs TIG welding without and with activated flux

fine-grained manipulation of weld properties is essential. Welders can precisely control penetration by modifying the flux’s chemical composition or flux delivery to suit the job at hand.

The addition of TiO₂ flux has resulted in a decrease in weld penetration depth when compared to the baseline A-TIG process without flux. The decrease in penetration can be explained by the inherent characteristics of TiO₂, which tend to redirect heat away from the weld pool, leading to

a shallower penetration. TiO₂ flux can be advantageous in scenarios where reducing heat input is paramount. The TiO₂ flux is helpful in welding scenarios where it is crucial to maintain a lower temperature to prevent distortion and overheating. This is particularly beneficial when working with thin materials or when avoiding excessive heat is vital. The reduced penetration of TiO₂ flux is advantageous for narrow groove welding applications that require precise control over the weld pool and minimal material distortion.

Fig. 6 Schematic illustration of Marangoni convection in **a** conventional TIG, **b** A-TIG welding process, direction of **c** Lorentz force, and **d** buoyancy force in the molten



The difference in penetration depth between TIG welding with and without flux is due to the Marangoni force, which is directed left and right without flux, as shown in Fig. 6a, and downward with flux, as shown in Fig. 6b, resulting in wider and shallower beads without flux and deeper and narrower beads with flux. In addition, a Lorentz force occurs due to a magnetic field, causing the weld pool to flow downward, as shown in Fig. 6c, and a buoyancy force occurs due to fluid density differences, as shown in Fig. 6d, which works upward with flux but is less effective for thin plates [18].

3.2 Tensile Test and Fracture of a Tensile Specimen of TIG and A-TIG Weldment

The tensile test was performed horizontally until the specimen is penetrated backward, with different welding currents used to achieve the same weld penetration for each flux variation. For example, welding without flux requires a higher welding current of 210 A, while welding with SiO₂, TiO₂, and NSN 308 fluxes require lower welding currents of 150, 160, and 180 A, respectively. Hence, welding with flux needs less heat input to achieve the same weld penetration, as observed from the macrostructural observations.

The results of the ultimate tensile strength (UTS) and elongation from each flux and base metal variation are given in Fig. 7. The study found that A-TIG welding with SiO₂ flux produces the highest UTS and elongation at 679.5 MPa and 70.3%, respectively. The use of flux positively affects the UTS of the weld, and SiO₂ flux, in particular, requires lower heat input to achieve the same penetration depth as welding without flux, resulting in deeper penetration and higher UTS. Welding with flux can produce superior tensile strength and elongation than welding without flux [2].

The fracture of the tensile test has occurred in the WM area. Scanning electron microscope (SEM) testing was carried out on the fracture surface of the tensile test specimen to

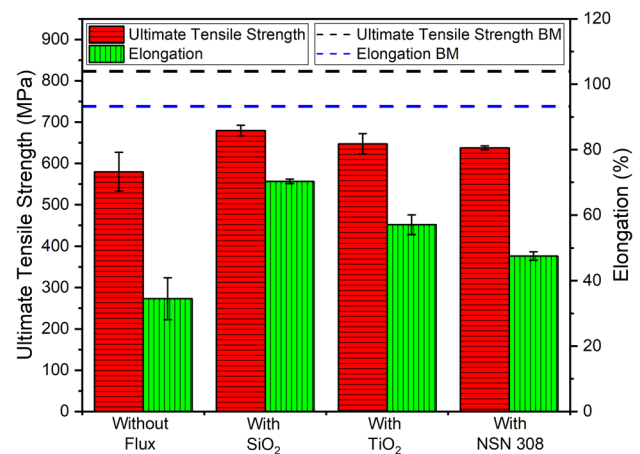
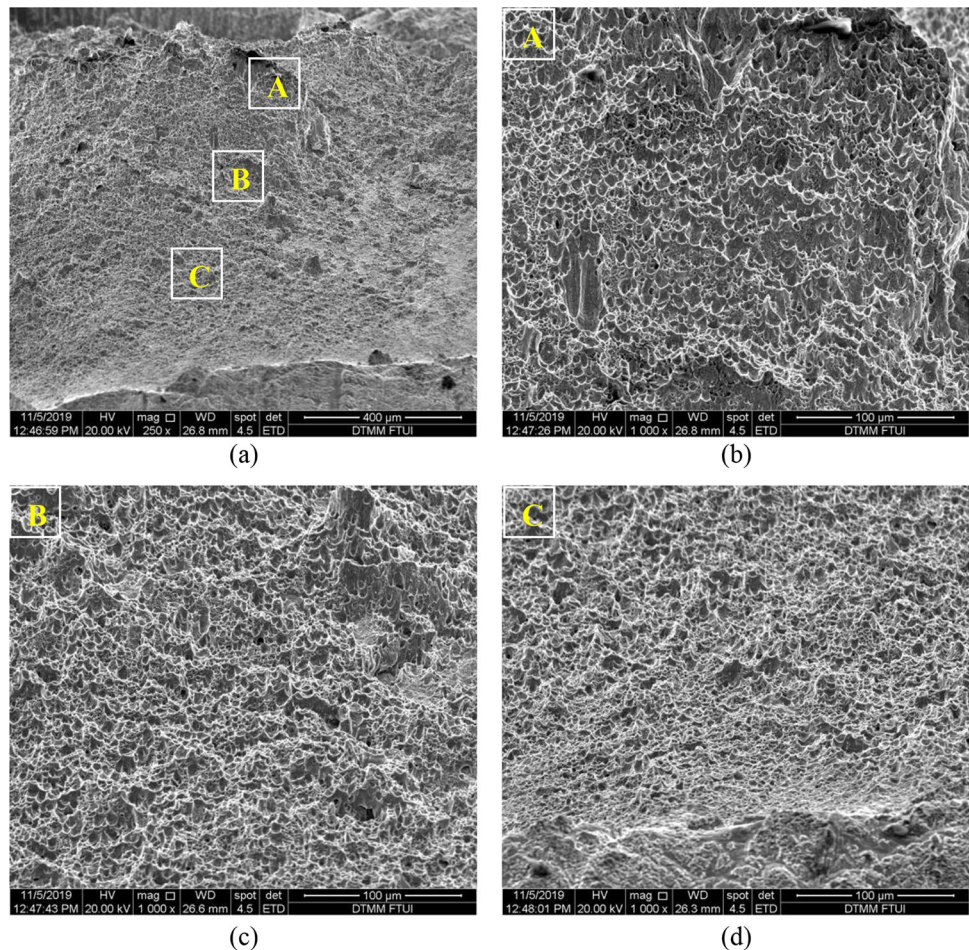


Fig. 7 Ultimate tensile test (UTS) on a various activated flux

determine the fracture structure. Figure 8a shows the fracture surface on NSN 308 activated fluxes. Welding with NSN 308 flux is seen in area A (Fig. 8b). The structure formed is a micro-void with relatively more ductile dimples. Furthermore, for area B the micro-void structure is still visible with smaller dimples than in area A (Fig. 8c). But in area C the dimples are still visible dimples formed (Fig. 8d).

A critical characteristic of a fracture surface is the presence of micro-voids. These tiny holes show where localized deformation and subsequent fracture have occurred. The fact that micro-voids in NSN 308-triggering fluxes suggests the occurrence of ductile deformation within the material. This is a desirable quality in applications where the welded joints must endure dynamic or impact stresses because it indicates a certain level of toughness and energy absorption capacity. The presence of larger and more ductile dimples in the micro-void structure highlights the material's ability for plastic deformation before breaking. The presence of dimples in the

Fig. 8 Fracture surface on NSN 308 activated flux with **a** low magnification, **b** high magnification in area A, **c** high magnification in area B and **d** high magnification in area C



material suggests that it can absorb energy, an essential characteristic for welds to endure stress and offer protection against potential failure.

The observation of varying dimple size and distribution across different regions of the fracture surface is a significant characteristic. The transition from area A to area B and subsequently to area C reveals interesting variations in dimple characteristics. The presence of smaller dimples in area B, as opposed to the larger ones in area A, suggests potential differences in the fracture mechanism. These variations might be influenced by factors such as variations in microstructure or stress distribution. The statement describes welding results with TiO_2 flux and NSN308 flux compared to SiO_2 flux. The micro-void structure is visible in all areas, but TiO_2 flux results in relatively more ductile dimples in areas A, B, and C, followed by NSN308 flux and then SiO_2 flux. The dimples formed in the fracture surface indicate a ductile failure mode in flux welding. Ahmadi et al. [12] reported that the fracture surfaces between welding without flux and welding with flux have dimple structures.

3.3 Microstructural Observation of TIG and A-TIG Weldment

Microstructure observations were made on cutting 2 (50%) of each flux variation and the BM. In the BM region, the austenite structure is dominated by large grain sizes. This is because the specimen used is SS 304 austenitic stainless steel.

Figure 9a shows microstructure TIG welding without flux in interface HAZ–WM area (i), HAZ region (ii), partially melted zone (PMZ) region (iii), and WM region (iv). In the HAZ, the grain size tends to be large due to more even heat distribution, causing longer grain growth times. In the PMZ, austenite dominates, and there are horizontal ferrite lines with vermicular morphology extending from the fusion boundary. The austenite grain size near the fusion boundary is larger than in the HAZ because it receives more heat from the hot weld metal. In the WM, δ -ferrite dominates in vermicular and lacy, and austenite is a secondary phase.

Figure 9b shows microstructure A-TIG welding with SiO_2 flux in interface HAZ–WM area (i), HAZ region (ii),

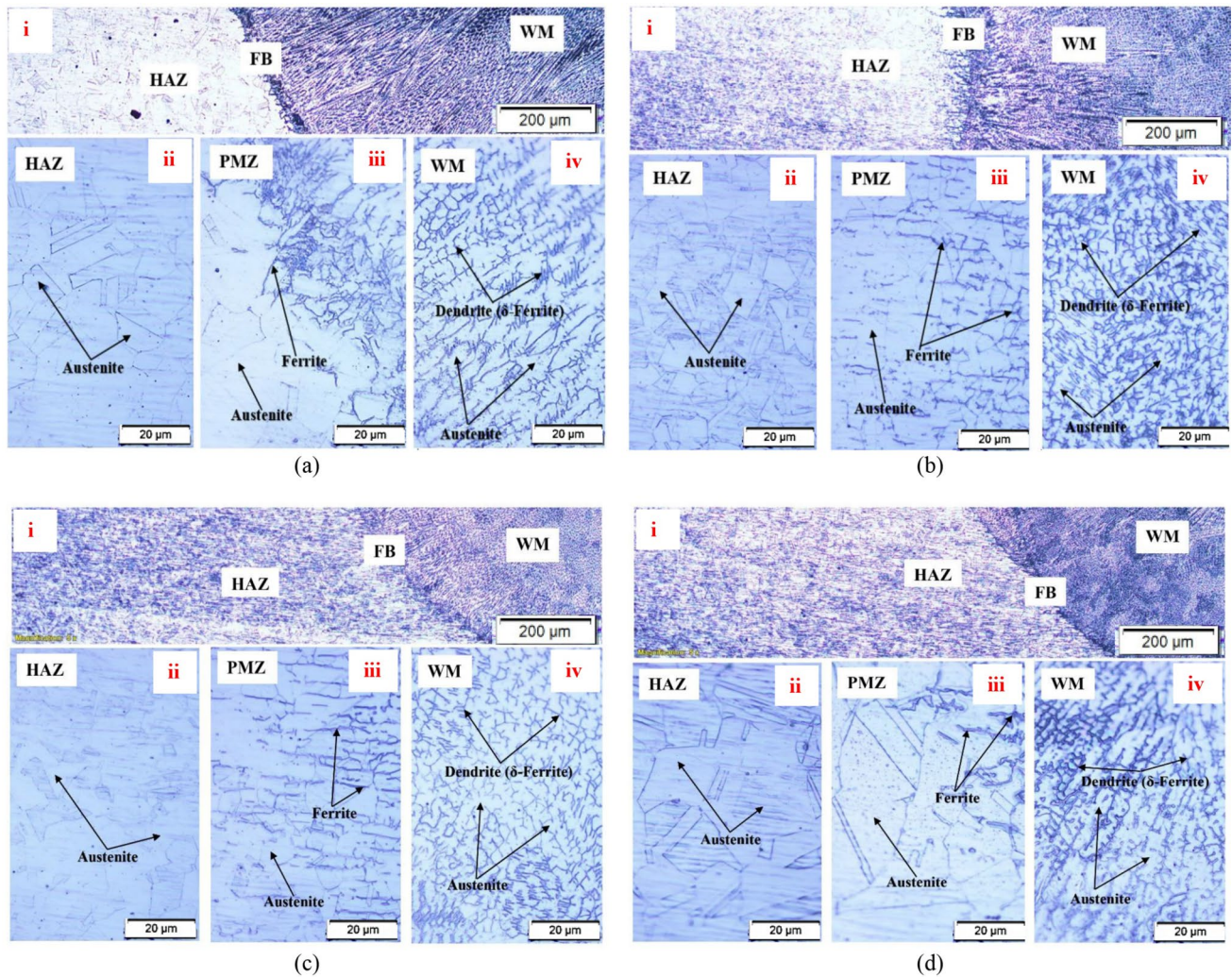


Fig. 9 Microstructure of TIG and A-TIG welding **a** without flux, **b** with SiO_2 , **c** with TiO_2 , and **d** NSN 308

PMZ region (iii), and WM region (iv). The grain size in the HAZ region of A-TIG welding with SiO_2 flux specimen is smaller than welding without flux. In the PMZ region, there are horizontal ferrite lines with vermicular morphology, and the amount of ferrite is higher in the SiO_2 flux specimen. The WM area is dominated by δ -ferrite, and the SiO_2 flux specimen has a higher amount of ferrite than welding without flux, indicating denser and darker ferrite lines.

Figure 9c shows microstructure A-TIG welding with TiO_2 flux in interface HAZ–WM area (i), HAZ region (ii), PMZ region (iii), and WM region (iv). The HAZ region of A-TIG welding with TiO_2 flux has a smaller grain size than welding without flux but is slightly larger than the SiO_2 flux welding result. The smaller grain size in welding without flux is due to more concentrated activating flux in the WM area, resulting in less heat distribution in the HAZ. On the other hand, the TiO_2 welding result has a larger grain size than the SiO_2 welding result, as the hot SiO_2 flux is more excellent

and penetrates deeper [20]. Therefore, the microstructure in the HAZ area is similar to A-TIG welding with SiO_2 flux. At the same time, δ -ferrite dominates the WM region with a vermicular shape, and some δ -ferrite lacy and austenite are seen as a secondary phase. Compared to welding without flux, TiO_2 flux results in lower δ -ferrite content in the WM area. This result is due to the smaller heat concentration in the WM area for TiO_2 flux, resulting in less δ -ferrite formation than WM in SiO_2 flux.

Figure 9d shows microstructure A-TIG welding with NSN 308 flux in interface HAZ–WM area (i), HAZ region (ii), PMZ region (iii), and WM region (iv). The NSN 308 flux welding specimen has a smaller grain size in the HAZ than welding without flux but larger than the SiO_2 and TiO_2 welding results. δ -ferrite dominates the WM region with a vermicular shape, and austenite is seen as a secondary phase. NSN 308 flux welding has a lower amount of δ -ferrite in the WM region than the other two fluxes. The NSN 308 flux

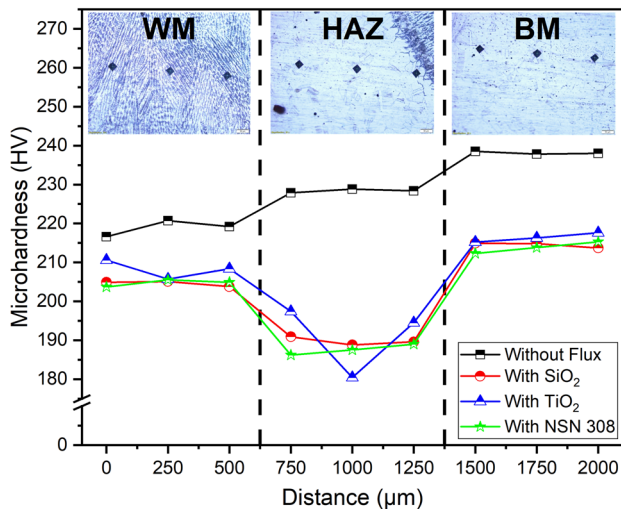


Fig. 10 Microhardness of horizontal distribution across WM, HAZ, and BM

is a rutile flux with TiO₂ as its main composition but with less oxide than pure TiO₂. The smaller amount of δ -ferrite formed in the WM region is due to the smaller heat concentration in this area for the NSN 308 flux.

Lu et al. [21] found that flux performance in increasing weld penetration is directly proportional to the amount of flux used. Thus, less oxide content results in shallower weld penetration. This result suggests that the heat concentration in the WM is less, and the cooling rate is the same. Therefore, with more significant heat input in the HAZ, the grain growth time is longer, resulting in relatively larger grains.

3.4 Microhardness Test of TIG and A-TIG Weldment

Microhardness measurements were conducted on the welds in three areas (BM, HAZ, WM), with three measurement points each. TIG welding without flux produces the highest microhardness value in each region, while welding with TiO₂ flux shows the lowest hardness value in the HAZ region. The results are shown in Fig. 10.

The microhardness of TIG welding without flux has been found to be highest at 221 HV in the WM region, while TiO₂ flux welding has the highest microhardness at 211 HV. The microhardness increases in the HAZ region in welding without flux with the highest value of 229 HV, but welding with flux decreases microhardness with the increased value of 198 HV in the TiO₂ flux type. This result is because welding with flux produces a smaller grain size in the HAZ region, leading to a difference in microhardness value in this region. In contrast, grain growth occurs in the WM region due to flux. As a result, finer grain is observed in welding with flux, so the microhardness in the WM region decreases compared to welding without flux [2].

4 Conclusions

In this experiment, the investigation of flux variations using A-TIG welding on stainless steel 304 has been successfully carried out. Based on the results of the data analysis, several conclusions can be drawn, including:

1. TIG welding with flux can produce a deeper weld penetration than without flux. The increase in weld penetration for SiO₂, TiO₂, and NSN308 fluxes was 89.9, 47.9, and 23.5%, respectively.
2. The ultimate tensile strength increases by 17.2% when using TIG welding with flux, while the increase in elongation is 103.7%. One of the reasons for increased tensile strength and elongation in TIG welding with flux is the difference in the D/W ratio.
3. TIG welding without flux produces higher microhardness than TIG welding with flux. The lowest microhardness is 198 HV using TiO₂ flux in the HAZ region.
4. Microstructure observation shows differences in the HAZ region, where TIG welding without flux has a larger grain structure, while TIG welding with flux has a finer grain structure. However, the microstructure formed for the WM region is almost the same for both methods.

Acknowledgements The authors would like to express their sincere gratitude for the financial support from Directorate Research and Public Service, Universitas Indonesia, with contract number NKB-1696/UN2.RST/HKP.05.00/2020.

References

1. Karunakaran, N. *International Journal of Engineering and Technology*, 2 (2012). [https://doi.org/10.1016/S1003-6326\(11\)60710-3](https://doi.org/10.1016/S1003-6326(11)60710-3)
2. Liu G-H, Liu M-H, Yi Y-Y, Zhang Y-P, Luo Z-Y, and Xu L, *Journal of Central South University* 22 (2015) 800. <https://doi.org/10.1007/s11771-015-2585-8>
3. Fujii H, Sato T, Lu S, and Nogi K, *Materials Science and Engineering: A* 495 (2008) 296. <https://doi.org/10.1016/j.msea.2007.10.116>
4. Adu E, and Danquah A, *International Journal of Scientific and Engineering* 7 (2016) 462.
5. Lucas B, *Welding and Metal Fabrication* 68 (2000) 7.
6. Baskoro A S, Fauzian A, Basalamah H, Kiswanto G, and Winarto W, *The International Journal of Advanced Manufacturing Technology* 99 (2018) 1603. <https://doi.org/10.1007/s00170-018-2552-2>
7. Nayee S G, and Badheka V J, *Journal of Manufacturing Processes* 16 (2014) 137. <https://doi.org/10.1016/j.jmappro.2013.11.001>
8. Modenesi P J, Apolinario E R, and Pereira I M, *Journal of materials processing technology* 99 (2000) 260. [https://doi.org/10.1016/S0924-0136\(99\)00435-5](https://doi.org/10.1016/S0924-0136(99)00435-5)

9. Vidyarthi R S, Dwivedi D K, and Vasudevan M, *Journal of Materials Engineering and Performance* **26** (2017) 1391. <https://doi.org/10.1007/s11665-017-2538-5>
10. Niagaj J, *Metals* **11** (2021) 530. <https://doi.org/10.3390/met11040530>
11. Touileb K, Ouis A, Djoudjou R, Hedhibi A C, Alrobei H, and Albaijan I, ... Abdo. H. S. *Metals* **10** (2020) 404. <https://doi.org/10.3390/met10030404>
12. Ahmadi E, and Ebrahimi A R, *Journal of materials engineering and performance* **24** (2015) 1065. <https://doi.org/10.1007/s11665-014-1336-6>
13. Pandolfi G S, Pinheiro Rodrigues F G, and Modenesi P, *J. Welding international* **32** (2018) 188. <https://doi.org/10.1080/09507116.2017.1347331>
14. Sivakumar, J., & Korra, N. N. *Arabian Journal for Science and Engineering*(2021), 1. <https://doi.org/10.1007/s13369-021-05409-w>
15. Sivakumar J, Vasudevan M, and Korra N N, *Transactions of the Indian Institute of Metals* **73** (2020) 555. <https://doi.org/10.1007/s12666-020-01876-1>
16. Vora J, Patel V K, Srinivasan S, Chaudhari R, Pimenov D Y, Giasin K, and Sharma S, *Metals* **11** (2021) 981. <https://doi.org/10.3390/met11060981>
17. Widyianto, A., Baskoro, A. S., & Kiswanto, G. *International Journal of Automotive and Mechanical Engineering*, 17 (2020), 7687. <https://doi.org/10.15282/ijame.17.1.2020.16.0571>
18. Vidyarthi R S, and Dwivedi D K, *Journal of Manufacturing Processes* **22** (2016) 211. <https://doi.org/10.1016/j.jmapro.2016.03.012>
19. Vora J J, and Badheka V J, *Transactions of the Indian Institute of Metals* **69** (2016) 1755. <https://doi.org/10.1007/s12666-016-0835-6>
20. Tanaka M, Shimizu T, Terasaki T, Ushio M, Koshiishi F, and Yang C L, *Science and technology of welding and joining* **5** (2000) 397. <https://doi.org/10.1179/136217100101538461>
21. Lu S, Fujii H, Sugiyama H, Tanaka M, and Nogi K, *Materials Transactions* **43** (2002) 2926. <https://doi.org/10.2320/matertrans.43.2926>

Publisher's Note Springer Nature remains neutral with regard to jurisdictional claims in published maps and institutional affiliations.

Springer Nature or its licensor (e.g. a society or other partner) holds exclusive rights to this article under a publishing agreement with the author(s) or other rightsholder(s); author self-archiving of the accepted manuscript version of this article is solely governed by the terms of such publishing agreement and applicable law.